Heliyon 10 (2024) e38021

Contents lists available at ScienceDirect

Heliyon

journal homepage: www.cell.com/heliyon

Research article

Shenqi Sanjie Granules induce Hmox1-mediated ferroptosis to inhibit colorectal cancer

Meng Chen [a,b,1], Shengli Ma [a,1], Wenbo Ji [b,c,1], Weihua Hu [d], Jiguang Gao [a], Jianke Yang [a], Yu Liu [b,c], Qianwen Cui [b,c], Shasha Yang [b], Xiaohui Xu [a,***], Haiming Dai [b,c,**], Lei Hu [a,b,*]

[a] School of Basic Medical Sciences, Wannan Medical College, Wuhu, 241002, China
[b] Anhui Province Key Laboratory of Medical Physics and Technology, Institute of Health and Medical Technology, Hefei Institutes of Physical Science, Chinese Academy of Sciences, Hefei, 230031, China
[c] University of Science and Technology of China, Hefei, 230026, China
[d] Reproductive Medicine Center, the First Affiliated Hospital of Wannan Medical College, Wuhu, 241001, China

ARTICLE INFO

Keywords:
Chinese herbal medicine
Shenqi Sanjie granules
Hmox1
Ferroptosis
Colorectal cancer
Quercetin
Luteolin
Kaempferol

ABSTRACT

Background: Because adverse reactions or drug resistance are often found after current chemotherapies for metastatic colorectal cancer (mCRC), new treatments are still in demand. Shenqi Sanjie Granules (SSG), an antitumor compound preparation of traditional Chinese medicine, has been recognized for its ability in clinical practice of oncotherapy. Nevertheless, the precise effects of SSG in colorectal cancer (CRC) and underlying mechanisms through which SSG inhibits CRC remain uncertain. The current study aimed to evaluate the anti-CRC activity of the Chinese herbal compound preparation SSG and investigate the underlying mechanisms of action.

Materials and methods: Initially, nine distinct cancer cell lines, including five CRC cell lines, one breast cancer cell line, two lung adenocarcinoma cell lines and one cervical cancer cell line, were used to evaluate the antitumor activity of SSG, and the mouse CRC cell line CT26 were used for further research. *In vitro* experiments utilizing diverse assays were conducted to assess the inhibitory effects of the SSG on CT26. Furthermore, subcutaneous syngeneic mouse model and AOM (azoxymethane)/DSS (dextran sodium sulfate) induced *in-situ* colitis-related mouse CRC model were used to evaluate the antitumor potential and biotoxicity of SSG *in vivo*. To elucidate the underlying molecular mechanisms, transcriptome sequencing and network pharmacology analysis were performed. Meanwhile, verification is carried out with quantitative real-time PCR (qRT-PCR) and flow cytometry (FCM) analysis.

Results: Our *in vitro* inhibition study showed that SSG could effectively inhibit CRC cell line CT26 growth and metastasis, and induce cell death. Neither of apoptosis inhibitor, necroptosis inhibitor, ferroptosis inhibitor, but the combination of the three diminished SSG-induced cell death, suggesting that multiple cell death pathways were involved. Both the syngeneic CRC model and the *in-situ* CRC model indicated SSG inhibited CRC *in vivo* with few toxic side effects. Further

* Corresponding author. School of Basic Medical Sciences, Wannan Medical College, Wuhu, 241002, China.
** Corresponding author. Anhui Province Key Laboratory of Medical Physics and Technology, Institute of Health and Medical Technology, Hefei Institutes of Physical Science, Chinese Academy of Sciences, Hefei, 230031, China.
*** Corresponding author. School of Basic Medical Sciences, Wannan Medical College, Wuhu, 241002, China.
E-mail addresses: xhxu@wnmc.edu.cn (X. Xu), daih@cmpt.ac.cn (H. Dai), huleiup@wnmc.edu.cn (L. Hu).
[1] M. Chen, S. Ma and W. Ji contributed equally to this work.

https://doi.org/10.1016/j.heliyon.2024.e38021
Received 21 May 2024; Received in revised form 4 September 2024; Accepted 16 September 2024
Available online 17 September 2024

mechanistic study suggested SSG treatment activated the ferroptosis pathway, particularly mediated by Hmox1, which was upregulated scores of times. Network pharmacology analysis indicated that the active ingredients of SSG, including Quercetin, Luteolin and Kaempferol were potential components directly upregulated Hmox1 expression.
Conclusions: Collectively, our findings indicate that the administration of SSG has the potential to inhibit CRC both *in vitro* and *in vivo*. The mechanism by which this compound preparation exerts its action is, at least partly, the induction of ferroptosis through upregulating Hmox-1 by its three active ingredients Quercetin, Luteolin and Kaempferol.

Abbreviations

SSG	Shenqi Sanjie Granules
Hmox1	heme oxygenease-1;
CRC	colorectal cancer
CAC	colitis-associated colon cancer
5-FU	5-fluorouracil
TKI	tyrosine kinase inhibitor
EGFR	epidermal growth factor receptor
ICI	immune checkpoint inhibitor
dMMR	deficient mismatch repair
ROS	reactive oxygen species
GPX4	glutathione peroxidase 4
TF	trasferrin
TFR1	transferring receptor 1
PUFA	polyunsaturated fatty acid
IC50	half-maximal inhibitory concentration
IHC	immunohistochemistry
H&E	haematoxylin/eosin
AOM	azoxymethane
DSS	dextran sulfate-sodium
GO	Gene Ontology
KEGG	Kyoto Encyclopedia of Genes and Genomes
DEG	differentially expressed gene
JC-1	5,5′,6,6′-tetrachloro-1,1′,3,3′-tetraethyl-imidacarbocyanine
DCFH-DA	2,7-dichlorodihydrofluorescein diacetate
DFC	2,7-dichlorofluorescein
GSH	γ-glutamylcysteinylglycine
PPI	protein-protein interaction
DAB	3,3′-Diaminobenzidine
OB	oral bioavailability
DL	drug-likeness
WBC	white blood cell
NEUT	neutrophilic granulocyte
LYMPH	lymphocyte
MONO	mononuclear leucocyte
RBC	red blood cell
HGB	hemoglobin
HCT	hematocrit
MCV	mean corpuscular volume
MCH	mean corpuscular hemoglobin
MCHC	mean corpusular hemoglobin concerntration
RDW-CV	red blood cell distribution width
PLT	platelets
PCT	thrombocytocrit
PDW	platelet distribution width
MPV	mean platelet volume

1. Introduction

Accompanied by the aging of population and changes in lifestyle, the annual incidence and mortality rates of colorectal cancer (CRC) are on the rise [1–3]. CRC is one of the most common malignant cancer in the digestive system, which are often diagnosed at late stages due to a lack of early symptoms [1–3]. Non-metastatic primary CRCs are typically removed surgically, whereas advanced recurrent or metastatic CRCs (mCRCs) may be treated with a combination of surgery, radiotherapy, chemotherapy, and other therapies. The 5-year survival rate is about 80–90 % for the primary CRC, while it is only about 10 % for the metastatic ones [3]. The chemotherapies for CRC mostly include 5-fluorouracil (5-FU) or other fluoropyrimidines, however, many patients develop resistance to 5-FU after it becomes refractory [4,5]. Irinotecan is used for patients with advanced CRC, however, its use and efficacy are limited due to severe adverse reactions, including diarrhea, dehydration, abdominal spastic pain, gastrointestinal injury and fever [6,7]. Oxaliplatin is commonly used in the late stage of CRC, though resistance and refractory cases are also common [7,8]. Several targeted therapies such as tyrosine kinase inhibitors (TKIs), antiangiogenic and anti-epidermal growth factor receptor (EGFR) agents have only limited or minor effects in mCRC in clinic [9–11], and immune checkpoint inhibitors (ICIs) are effective only in mCRCs with deficient mismatch repair (dMMR), which account for about 5 % of mCRC cases [12–14]. Thus, there is an urgent need to explore alternative treatments for mCRC.

Chinese herbal medicine represents an important resource for discovering and developing anti-cancer compounds. Among these Chinese herbal medicines, some monomer extracts including alkaloids, terpenoids, flavonoids, quinines, and steroids, have been shown to inhibit cancer by regulating cancer cell division, proliferation, apoptosis, invasion and metastasis, inhibiting tumor neovascularization, and modulating anti-cancer immune response [15–18]. Compound herbal preparations are also widely utilized in cancer research and treatment, including for CRC [15–18]. However, the complexity of their composition often results in a lack of clarity regarding their pharmacological mechanisms, toxicity assessments, and safety evaluations, which limits their clinical application [18]. With the advent of recent technological advancements, exploring and analyzing the pharmacological mechanisms of Chinese herbal medicine and its components is now feasible.

Ferroptosis is a form of necrosis induced by iron-dependent excessive levels of reactive oxygen species (ROS) and lipid peroxides, which damage the inner side of the cell membrane. Several mechanisms, including disruption of the iron homeostasis, accumulation of lipid peroxides, and reduction of glutathione peroxidase 4 (GPX4) activity, have been identified to induce ferroptosis [19–24]. Various genes or proteins regulating iron homeostasis have been shown to modulate ferroptosis. For example, Fe^{3+} mainly transfers into the cell by endocytosis through combination with transferrin (TF) and transferring receptor 1 (TFR1) complex and enters the lysosome,

where Fe^{3+} will be released and converted into Fe^{2+} through the action of iron reductase STEAP3 and released into the cytoplasm [25,26]. Excessive levels of Fe^{3+} in the cells, which either caused by increased importation or reduced transformation to Fe^{2+}, will induce ferroptosis. Upregulation of heme oxygenease-1 (Hmox1), which is the rate limiting enzyme in the process of heme catabolism of iron porphyrin compound and thus control the heme decomposition of Fe^{2+}, will also induce or promote ferroptosis [27–29]. PUFAs (polyunsaturated fatty acid), which are important components of the bilayer of phospholipids in cell membranes to maintain the fluidity of cell membrane, when excessive will generate hydroxyl radicals through Fenton reaction, producing a large amount of peroxides and leading to ferroptosis [30]. The inhibition of GPX4 induces ferroptosis because it reduces lipid peroxides and inhibits the occurrence of lipid peroxidation [20,31].

Previous studies have shown that the anti-tumor mechanism of some Chinese herbal medicine is closely related to the induction of ferroptosis. Piperonamide, an alkaloid largely exists in the long pepper (Piper longum L.), induces cancer cell ferroptosis by upregulating ROS level [32,33]. Tagitin C, a sesquiterpene lactone isolated from Tithonia diversifolia, induces ferroptosis in CRC cells through the ER stress and downstream PERK-Nrf2-Hmox1 signal pathway [34]. Sorafenib, altretamine and other drugs used clinically can also induce ferroptosis and promotes tumor treatment [35]. Although a large number of studies have shown that intervention of Chinese herbal medicine can effectively reduce the complications of CRC patients and reduce the recurrence rate and metastasis rate of tumors, there is still a lack of research on Chinese herbal medicine inducing ferroptosis of CRC [36].

In the present study, we found that the traditional Chinese herbal remedy Shenqi Sanjie Granules (SSG, 5 g Jianghuang/turmeric, 3 g Kushen/lightyellow sophora root, 1.5 g Renshen/ginseng, 1.5 g Huangqi/milkvetch root, 4.5 g Gancao/licorice, and 7.5 g Dasuan/garlic, Table S1) effectively promoted CRC death and inhibited the proliferation and migration of the cells. Moreover, it significantly impeded the growth of subcutaneous syngeneic CRC tumors and in-situ induced CRC tumors in mice without affecting the health of mice. These findings are in concert with contemporary pharmacological insights that underscore the diverse anticancer benefits of these herbs. Turmeric, recognized for its potent anticancer profile, has been extensively investigated due to its capacity to suppress cell proliferation, trigger apoptosis, and regulate pathways pivotal to cancer development, while its antioxidant properties are currently under scrutiny for their potential role in instigating ferroptosis [37]. Ku Shen exerts its anti-cancer effects by inhibiting cell growth and inducing apoptosis through the regulation of key signaling cascades, including MAPK, JAK-STAT, NF-κB, Wnt/β-catenin, and mTOR [38]. Ren Shen, revered for its adaptogenic and immune-enhancing properties, is being explored for its potential to combat cancer, with ginsenosides demonstrating the ability to suppress tumor growth and induce apoptosis by modulating cell cycle and apoptotic pathways [39]. Huang Qi, a fundamental herb in traditional Chinese medicine, is esteemed for bolstering immunity and alleviating inflammation, with its constituents—Astragalus polysaccharides and flavonoids—showing promise in cancer therapy by regulating BMSCs and cytokines, thereby inhibiting tumor growth and inducing apoptosis [40]. Recent *in vitro* and *in vivo* studies comprehensively reveal that licorice extracts and purified compounds possess anticancer properties through various mechanisms, including proliferation inhibition, cell cycle arrest, apoptosis, autophagy, differentiation, metastasis and angiogenesis suppression, as well as chemotherapy and radiotherapy sensitization, and their combined use with clinical chemotherapy drugs significantly boosts anticancer effects while mitigating side effects [41]. Garlic's potential to induce ferroptosis is a subject of ongoing research, with initial studies indicating its capacity to perturb iron homeostasis within cancer cells [42]. To further elucidate the molecular mechanism of anti-tumor effect of SSG, we conducted transcriptome sequencing and network pharmacology analyses. The results indicated that the active monomers, Quercetin, Luteolin and Kaempferol, of SSG directly upregulated Hmox1 expression to induce ferroptosis.

2. Materials and Methods

2.1. Ethics statement

All animal experiments were performed according to the guidelines of the Animal Use and Care Committees at the Hefei Institutes of Physical Science, Chinese Academy of Sciences (approval number, SWYX-DW-2021-74; approval date, 10/25/2021).

2.2. Preparation of Shenqi Sanjie granules

Shenqi Sanjie Granules (SSG), an antitumor compound preparation of traditional Chinese medicine which has been for clinical practice for many years in the Yong Ji Sheng He Geriatric Hospital, Jilin, Jilin, China. Each SSG contains 5 g Jianghuang/turmeric (Sichuang, China), 3 g Kushen/lightyellow sophora root (Jilin, China), 1.5 g Renshen/ginseng (Jilin, China), 1.5 g Huangqi/milkvetch root (Neimenggu, China), 4.5 g Gancao/licorice (Xinjiang, China), and 7.5 g Dasuan/garlic (Shandong, China). Briefly, Jianghuang, Kushen, Renshen, Huangqi and Gancao were soaked in 10 times of water for 30 min, then bring to a boil with strong fire, and followed by simmer for 60 min. Then Dasuan in 1 mm thick slices were added and the mixture was boiled for another 5 min. The residue was then removed by filtration, and the obtained drug solution was dehydrated by vacuum distillation dehydration. The powder was then prepared as a stock solution (100 mg/mL) with DMSO for cell treatment and distilled water for intragastric administration respectively, and stored at −80 °C.

2.3. Cell culture and cell treatment

The mouse colon cancer cell line CT26 and the human breast cancer cell line MDA-MB-231 were kind gifts from Dr. Qingsong Liu (Hefei Institutes of Physical Science, Chinese Academy of Sciences (CASHIPS)). The human lung adenocarcinoma cell lines PC-9 and H1299 were kindly gifted from Wei Han (CASHIPS). The human cervical cancer cell line HeLa was obtained from Xin Ye (Institute of

Microbiology, Chinese Academy of Sciences) and the human colon cancer cell line HCT116 was gifted from Scott H. Kaufmann (Mayo Clinic, Rochester, MN). The human colon cancer cell lines HT29, LOVO and SW620 were purchased from Ubigene Biosciences (Guangzhou, China). Cell characterization (polymorphic short tandem repeat profiling) and contamination tests were performed. CT26 cells and H1299 cells were cultured in RPMI-1640 medium (SH30809.01, HyClone), MDA-MB-231 cells, PC-9 cells, HeLa cells HT29 cells, LOVO cells and SW620 cells were maintained in DMEM (SH30243.01, HyClone) and HCT116 cells was grown in McCoy's 5A (16600082, Gibco). All cells were cultured at 37 °C with 5 % CO_2, supplemented with 10 % FBS (fetal bovine serum, FB25015, Clark) and 1 % PS (penicillin-streptomycin, SV30010, Hyclone).

For cell treatment, cells were pre-seeded overnight until cell density reached ~60 %. The culture medium was switched to fresh medium containing SSG with specified concentrations and then incubated for a period of time as indicated. To identify the death signaling pathway induced by SSG, 50 μM Q-VD-OPh (QVD, a pan-caspase inhibitor, HY-12305, MedChemExpress), Ferrostatin-1 (Fer-1, a ferroptosis inhibitor, HY-100579, MedChemExpress) and Necrosulfonamide (Nec, a necroptosis inhibitor, HY-100573, MedChemExpress) were pre-incubated with CT26 cells for 1 h alone or together before adding SSG.

For Hmox-1 knockdown, two individual siRNAs targeting the *Hmox-1* gene and nontargeting control siRNA were purchased from GenePharma (Shanghai, China). The sequences of siHmox-1 #1 and siHmox-1 #2 were 5′-UGGAUGUGUACCUCCUUGTT-3′ and 5′-CUCUAUCGUGCUCGAAUGAA-3′, respectively. The sequence of siControl was 5′-UUCUCCGAACGUGUCACGUTT-3'. To perform the knockdown assay, 6×10^5 CT26 cells were plated in a 6-well plate. 24 h post-seeding, 80 pmol of siRNAs were transfected using Lipofectamine RNAiMAX (13778–075, Invitrogen) following the manufacturer's instructions. In brief, 80 pmol of siRNA and 8 μL of RNAiMAX were each diluted in 200 μL of Opti-MEM (31985–070, Gibco) serum-free medium. After a 15 min incubation, the siRNAs were transferred to the RNAiMAX and mixed gently. Following an additional 15 min room temperature incubation, the mixtures were added to the cells and incubated for 8 h. The medium was then replaced with fresh RPMI-1640 medium supplemented with 10 % FBS and 1 % PS, and the cells were maintained at 37 °C with 5 % CO_2 for further treatment.

2.4. Cell counting Kit-8 (CCK-8) assay

The half-maximal inhibitory concentration (IC50) values of various cancer cell lines were determined by CCK-8 (C0039, Beyotime) assay according to the manufacturer's instructions. Briefly, 10,000 cells were seeded into a 96-well plate. 24 h later, various concentrations (0, 4, 8, 16, 24, 32, 48, 64, 128, 256 μg/mL) of SSG were added to the medium and treated for another 24 h 10 μL CCK-8 solution was then added and incubated for 2 h at 37 °C with 5 % CO_2, and absorbance at 450 nm was measured using CMax Plus (Molecular Devices, LLC). The IC50 values were generated by GraphPad Prism 5. Each sample was tested in triplicates to obtain the average. Data were shown as means ± (standard deviation) SD.

10,000 CT26 cells were seeded on 96-well plate before 50 μg/mL SSG treatment, and 10 μL CCK-8 solution was added and incubated for 2 h after indicated time (0, 6, 12, 24, 48 h). Absorbance at 450 nm was also measured and calculated according to the following formula to determine the cell viability: Cell viability (%) = (ODsample - ODblank)/(ODControl - ODblank) × 100. Each sample was tested in triplicates and data were shown as means ± SD.

2.5. Colony formation assay

200 CT26 cells were seeded into 6-well plate, and after 48 h, the medium was replaced by fresh RPMI-1640 supplemented with 10 % FBS and 1 % PS with 2 μg/mL SSG for 2 weeks. Then the cells were washed two times with PBS and fixed in cold methanol for 30 min. 0.5 % (w/v) crystal violet was used to stain the fixed colonies for another 30 min at room temperature. Residual crystal violet was rinsed away with PBS. And then, the areas of cell colonies were analyzed by Image J software. Each experiment was repeated three times and data were shown as means ± SD.

2.6. Wound healing assay

Each well of 6-well plate was seeded 8×10^5 CT26 cells. About 30 h later (cells confluence reached 100 %), 200-μL sterile pipette tips were used to scratch the wound uniformly. Then the wells were washed three times with PBS to remove cell debris and replaced by fresh serum-free RPMI-1640 with 2 μg/mL SSG. After a certain time (0, 24, 48, 72 h), images at specific wound sites were taken under a microscope (Olympus CKX53) and the width of the wound was measured by Image J software. Each experiment was conducted in triplicate and data were shown as means ± SD.

2.7. Haematoxylin/eosin (H&E) staining

Collected tissues including livers, spleens, stomachs and kidneys were fixed in 10 % formalin and then embedded in paraffin. Whereafter, the tissues were cut into 5-μm-thick sections for H&E staining. Briefly, tissue slices were dewaxed in xylene, rehydrated through graded ethanol to water, stained with the H&E kits (G1120, Solarbio) step by step, then dehydrated, transparentized, and sealed. After staining, the tissue slices were observed using Olympus CKX53 and images were captured by TCapture software.

2.8. Immunohistochemistry (IHC)

The immunohistochemical staining for Ki67/cleaved Caspase-3/Hmox-1 was done according to standard protocol. Briefly,

paraffin-embedded, formalin fixed tissue sections were deparaffinized in a gradient solution of xylene and then rehydrated in pure ethanol and PBS buffer. Then, 0.1 M citrate buffer (pH 6.0) was used to repair the antigenic epitope at 95 °C for 20 min and subsequently blocked with 10 % goat serum for 60 min. The tissues in slides were then incubated overnight with the diluted Ki67 (9449, Cell Signaling Technology)/cleaved Caspase-3 (9664, Cell Signaling Technology)/Hmox-1 (A19062, ABclonal) antibody at 4 °C, afterward washed three times with PBS and incubated with secondary antibody followed by DAB (3,3′-Diaminobenzidine) staining (abs998, Absin Bioscience). After counterstaining with haematoxylin (abs998, Absin Bioscience) and mounting with mounting medium, slides were visualized and captured under a bright-field microscope using Olympus CKX53 with TCapture software. The expression level of Ki67/cleaved Caspase-3 was determined by IPP 6.0 (Image Pro Plus 6.0) in blinded experiments for statistical analysis.

2.9. RNAseq analysis

After being treated with DMSO or SSG for 6 h, CT26 cells were harvested and washed three times with cold PBS. Then the cell pellets in triplicates for each group were sent to Novogene (Beijing, China) in dry ice for transcriptome sequencing. Raw reads were trimmed to remove low-quality bases and adaptor sequences using fastp (default parameters). Reference genome and gene model annotation files were downloaded from genome website directly. Index of the reference genome was built and paired-end clean reads were aligned to the reference genome using Hisat2 v2.0.5. Differential expression analysis of two groups was performed using DESeq2 R package (1.20.0). The resulting *p*-value were adjusted using the Benjamini and Hochberg's approach for controlling the false discovery rate. Genes with an adjusted *p*-value$\leq$0.05 found by DESeq2 were assigned as differentially expressed. Then the differentially expressed genes were collected to performed GO enrichment analysis and KEGG analysis by the clusterProfiler R package, and Protein-Protein Interactions (PPI) analysis based on the STRING database.

2.10. Quantitative real-time polymerase chain reaction

After treating with SSG for indicated time (0, 1, 3, 6 h), total CT26 cells were harvested and washed three times with cold PBS. Then total RNA was extracted according to the EasyPure® RNA Kit (ER101, TransGen Biotech) and subjected to reverse transcription using reverse transcription kit (AT311-02, TransGen Biotech), and followed by detection using PerfectStart® Green qPCR SuperMix (AQ602-11, TransGen Biotech). The gene-specific primers were as follows: *Hmox-1* forward, 5′-AAGCCGAGAATGCTGAGTTCA-3′ and reverse, 5′-GCCGTGTAGATATGGTACAAGGA-3'; *Ddit3* forward, 5′-CACCTATATCTCATCCCCA-3′ and reverse, 5′-GGATGTGCGTGTGACCTCT-3'; *IL-6* forward, 5′-GAGGATACCACTCCCAACAGACC-3′ and reverse, 5′-AAGTGCATCATCGTTGTTCATACA-3'; *DUSP1* forward, 5′-CAGGAAGGACAGGATCTCCA-3′ and reverse, 5′-CTGTGCAGCAAACAGTCCAC-3'; *Ptgs2* forward, 5′-TGCCTGGTCTGATGATGTATG-3′ and reverse, 5′-GGGGTGCCAGTGATAGAGTG-3'; *Sqstm1* forward, 5′-TGTGGAACATGGAGGGAAGAG-3′ and reverse, 5′-TGTGCCTGTGCTGGAACTTTC-3'; *GPX4* forward, 5′-TAAGAACGGCTGCGTGGTGAAG-3′ and reverse, 5′-AGAGA-TAGCACGGCAGGTCCTT-3'; *Nrf2* forward, 5′-TAAAGCTTTCAACCCGAAGCACGC-3′ and reverse, 5′-TACAGTTCTGGGCGGCGACTT-TAT-3'; *GAPDH* forward, 5′- AATGGTGAAGGTCGGTGTGAAC-3′ and reverse, 5′-GCCTTGACTGTGCCGTTGAA-3'. Samples were amplified by Roche 480 Light Cycler (Roche, Basel, Switzerland) and the data analysis was performed with the $2^{-\Delta\Delta Ct}$ method.

2.11. Measurement of mitochondrial membrane potential with JC-1 staining

Mitochondrial membrane potential was determined using the Mitochondrial membrane potential assay kit with JC-1 (S2006, Beyotime Biotechnology) according to the manufacturer's instruction. Briefly, for fluorescence detection, CT26 cells were cultured in a 6-well plate and treated with SSG for 0, 1, 3 or 6 h. After treatment, cells were rinsed and then incubated with 300 μL of JC-1 staining working solution at 37 °C for 20 min in darkness. Following two washes with PBS, cells were visualized using fluorescence microscopy (ECLIPSE Ts2R, Nikon). Mean fluorescence intensity was determined using Image Pro Plus 6.0 software, and results were presented as the ratio of red/green fluorescence intensity.

2.12. Reactive oxygen species (ROS) measurement

To measure the intracellular ROS, fluorescent probe DCFH-DA (S0033S, Beyotime Biotechnology) was used according to the manufacturer's instruction. After being treated with SSG for 0, 1, 3 or 6 h, DCFH-DA solution (10 μM) was added and incubated for 30 min at 37 °C in dark. Then the cells were harvested and washed three times with PBS, and followed by detection using CytoFLEX (Beckman Coulter) and analysis by FlowJo analysis software (TreeStar, Ashland, OR, USA).

2.13. Measurement of malondialdehyde (MDA) levels

Levels of MDA in both control and SSG treated CT26 cells were detected with Lipid Peroxidation MDA Assay Kit (S0131S, Beyotime, Shanghai, China) following the manufacturer's instructions. Each group was conducted in triplicate.

2.14. Network pharmacology analysis

To better understand the potential mechanism, SSG was analyzed using Network pharmacology. Briefly, traditional Chinese medicine systems pharmacology database and analysis platform (TCMSP, https://tcmspw.com/tcmsp.php) was used to retrieve active

ingredients of SSG and predict the targets of active ingredients. The active ingredients satisfied both oral bioavailability (OB) ≥ 30 % and drug-likeness (DL) ≥ 0.18 were collected. At the same time, the targets of active ingredients were also predicted using TCMSP, while the UniProt database (https://www.uniprot.org/) was used to standardize the drug target of human species of each active ingredient. Then the targets related to CRC were obtained through retrieving the OMIM (https://omim.org/search/advanced/), GeneCards (https://www.genecards.org/) and PharmGKB (https://www.pharmgkb.org/) database search using the keyword "colorectal cancer". The online jvenn (http://jvenn.toulouse.inra.fr/app/index.html) was used to map drug targets and CRC targets and to get the intersection targets. For PPI (protein-protein interaction) network construction, the intersection targets were imported into the STRING database (https://string-db.org/cgi/input). The confidence ≥0.4 was set and the free nodes were hidden. Cytoscape 3.9.0 software was then used to process the PPI network to realize visualization and screen out the core targets. For GO (Gene Ontology) and KEGG (Kyoto Encyclopedia of Genes and Genomes) enrichment analysis of the screened core targets, the DAVID data platform (https://david.ncifcrf.gov/tools.jsp) was used, and then the bioinformatic online platform (https://www.bioinformatics.com.cn/) was used to visualize the result analysis. For constructing the "active ingredients-core targets" network, the Cytoscape 3.9.0 software was used.

2.15. Animal experiments

All animal experiments protocols were performed in accordance with P.R. China legislation for the use and care of laboratory animals. The animal care and study protocols were authorized by the Animal Use and Care Committees at the Hefei Institutes of Physical Science, Chinese Academy of Sciences (approval number, SWYX-DW-2021-74). All Balb/c mice (5-week old) were purchased from GemPharmatech (Nanjing, China) and maintained in a specific pathogen-free environment. The mice were kept at a constant temperature (25 ± 2 °C) with controlled illumination (12 h light/dark cycle), and free access to food and water. The mice were acclimated to the environment for one week before being subjected to further treatment.

For syngeneic tumor assay, 5×10^5 CT26 cells in 100 μL PBS were injected subcutaneously under the shoulder of eight mice per group, and then the mice were divided randomly into two groups. 0.5 g/kg SSG in 150 μL distilled water or an equal volume of physiological saline (0.9 % NaCl) for each mouse (≈22–25 g) was intragastric administration twice a day. The body weight and the tumor volume were respectively weighed with electronic balance and vernier caliper every three days, and the volume was calculated as $(D^2 \times d)/2$, where D was the large diameter and d is the small diameter of the tumor. When tumors reached a volume of about 2000 mm^3, blood was collected from the orbit for further haematological analysis, and closely followed by execution by neck amputation. The tumors and tissues including livers, spleens, stomachs and kidneys were segregated, measured and stored at −80 °C for later use.

Male Balb/c mice were used to induce colitis-associated colon cancer (CAC) because males are more prone to CRC than females and to avoid any effects due to female hormones or estrus cycle. To establish the CAC model, each mouse was intraperitoneally injected with 10 mg/kg of azoxymethane (AOM) dissolved in PBS. One week later, these mice received 3 % dextran sulfate-sodium (DSS) in the drinking water for 7 days, followed by regular drinking water for recovery thereafter. After three rounds of 3 % DSS treatment, the mice were randomly divided into two groups to be given SSG or equal volume of 0.9 % NaCl once a day by gavage for eight weeks. Mice were weighed weekly and sacrificed at the end of the 15th week. Take blood from the orbit for haematological analysis, and collect colonic tissues and livers, spleens, stomachs and kidneys for further analysis.

2.16. Haematological analysis

Collected blood were stored in 0.5 mL microtainers ethylenediaminetetracetic acid (K2-EDTA, BD, USA) and analyzed using the ABX Micros 60 (Horiba ABX, Montpellier, France). The following blood cells were counted and calculated: white blood cell (WBC), neutrophilic granulocyte (NEUT), lymphocyte (LYMPH), mononuclear leucocyte (MONO), red blood cell (RBC), hemoglobin (HGB), hematocrit (HCT), mean corpuscular volume (MCV), mean corpuscular hemoglobin (MCH), mean corpusular hemoglobin concerntration (MCHC), red blood cell distribution width (RDW-CV), platelets (PLT), thrombocytocrit (PCT), platelet distribution width (PDW), mean platelet volume (MPV). Values are expressed as mean ± SD. *P* values were obtained from unpaired 2-tailed Student *t*-test. Clinical indexes with significant differences ($P < 0$ 0.05) are in bold.

2.17. Statistical analysis

All the statistics were shown as the means ± SD. The number of replicates for each experiment was indicated in the figure legends. The statistical differences between the two groups were evaluated using a 2-tailed *t*-test, and the R software and GraphPad Prism 5 were utilized to perform the statistical analysis. $P > 0.05$ was considered not significant (ns). *$P < 0.05$, **$P < 0.01$, ***$P < 0.001$.

3. Results

3.1. SSG inhibits CRC cells through multiple mechanisms

To investigate the effect of SSG on cancer cells, we first used viability assay to assess its abilities to inhibit cell growth in nine distinct cancer cell lines, including the mouse CRC and human CRC cell lines CT26, SW620, HT29, LOVO and HCT116, the human cervical cancer cell line HeLa, the human breast cancer cell line MDA-MB-231, and the human lung cancer cell lines PC-9 and H1299. We found the CT26 cell line was the most sensitive to SSG with an IC50 of 40.98 μg/mL, while the IC50s for other CRC cell lines SW620,

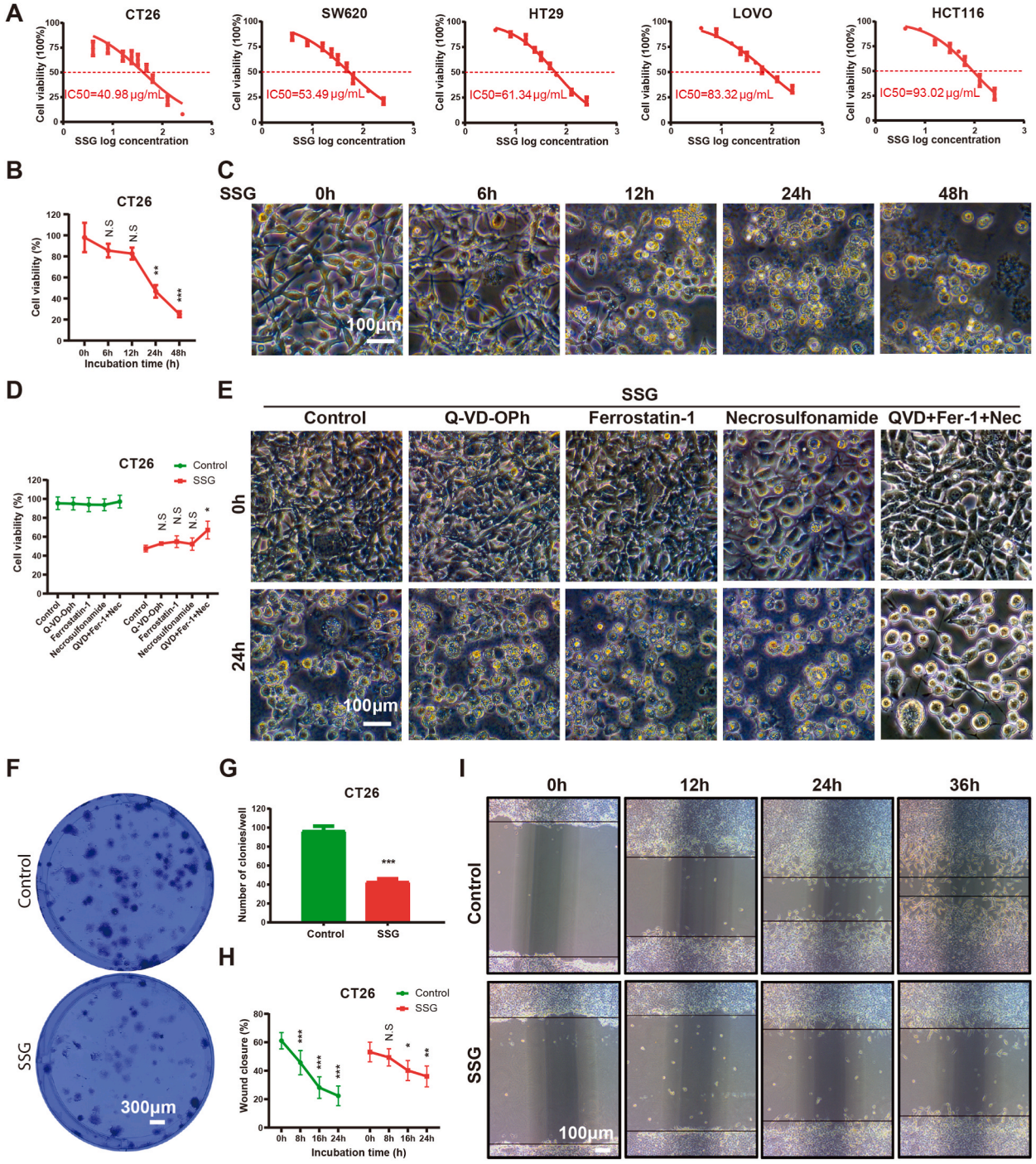

Fig. 1. SSG inhibits CRC through multiple pathways. (A) After CRC cell lines CT26, SW620, HT29, LOVO and HCT116 were treated with increasing concentrations of SSG (0–1000 μg/mL), cell viability was analyzed by CCK-8 staining to determine the IC50. Error bars, means ± SD (*$p < 0.05$, **$p < 0.01$, ***$p < 0.001$ versus control, $n = 3$ independent experiments), similarly hereinafter. (B–C) After CT26 cells were treated of SSG (1000 μg/mL) for the indicated time, cell viability was analyzed by CCK-8 staining (B) and morphology was captured (C). (D–E) After CT26 cells were treated with DMSO, Q-VD-OPh (QVD), Ferrostatin-1 (Fer-1), Necrosulfonamide (Nec), or the combination of QVD, Fer-1 and Nec for 1 h, cells were then treated with SSG (1000 μg/mL) for 24 h, cell viability (D) was analyzed and morphology was viewed (E). (F–G) 200 CT26 cells were plated and incubated with DMSO or SSG (2 μg/mL) for 2 weeks. A representative experiment (F) and the summary results from three independent experiments (G) were shown. (H–I) 8×10^5 CT26 cells were plated into 6-well plate to perform a wound-healing assay. Representative images were obtained at the indicated time points, and the results were quantified with Image J software.

HT29, LOVO and HCT116 were 53.49 μg/mL, 61.34 μg/mL, 83.32 μg/mL and 93.02, respectively (Fig. 1A). These IC50 values, being lower in comparison to other tumor cell types (Fig. S1), indicated SSG's selective cytotoxicity across various tumor types.

Since CT26 cells were the most sensitive to SSG, CT26 cells were used to evaluate SSG effects and the molecular mechanisms in our further experiments. SSG induced a time-dependent decreases of viability (Fig. 1B) and a time-dependent cell death in CT26 cells, as more cells floated and showed round and shrinkage morphologies when the incubation time increases (Fig. 1C). To find out which type of cell death were induced, the pan-caspase inhibitor Q-VD-OPh, the ferroptosis inhibitor Ferrostatin-1, the necroptosis inhibitor Necrosulfonamide, or a combination of the three were added 1 h before SSG treatment (Fig. 1D and E). While each of these inhibitors did not affect SSG-induced morphology and viability decrease, however, a combination of the three increased the viability and inhibited the morphology changes significantly (Fig. 1D and E), suggesting that multiple cell death pathways were involved. Further colony formation assay (Fig. 1F and G) and cell migration assay (Fig. 1H and I) suggested that SSG not only inhibited tumor cell proliferation, but also suppressed its metastasis. Thus, SSG inhibited CRC cells through multiple mechanisms.

3.2. SSG inhibits syngeneic tumors of CRC while the mice are tolerable

To test the therapeutic potential of SSG *in vivo*, a subcutaneous syngeneic mouse model of CT26 cells was established (Fig. 2A). Each mouse was inoculated with 5×10^5 CT26 cells followed by the treatment with SSG or vehicle control by stomach irrigation. These studies showed that SSG significantly inhibits the tumor growth (Fig. 2B–D). To further investigate the underlying molecular mechanism, we used IHC staining to determine the cell proliferation marker Ki-67, the apoptosis marker cleaved Caspase-3, and the Hmox-1, which is known to induce ferroptosis when excessively upregulated [19], in the tumor tissue sections from SSG-treated and vehicle control mice. We found significantly decreased Ki-67 expression and increased expressions of cleaved Caspase-3 and Hmox-1 in the SSG-treated group compared to the vehicle group (Fig. 2E–J). These findings suggest that SSG inhibited tumor cell growth and also promoted tumor cell death via multiple death signaling pathways *in vivo*, consistent with the *in vitro* results. To evaluate the tolerability of SSG, we measured mice weight, performed the histopathological analysis of multiple organs, and counted the blood cells from these mice. Compared to control group, SSG did not reduce mice weight significantly (Fig. 2K) and no signs of cytotoxicity were found in stomach, liver, kidney, and spleen (Fig. 2L), indicating tolerability of the treatment. Moreover, SSG treatment significantly increased the percentage of NEUT% and reduced the amount of Lymph%, indicating that the inflammation may be induced in the transplanted tumors (Table S2). Taken together, these data indicated that SSG inhibits CRC syngeneic tumors *in vivo* while the mice are tolerable to the treatment.

3.3. SSG inhibits CRC growth in an in-situ mouse model

To further simulate CRC *in-situ* and test the therapeutic potential of SSG, we also built an *in-situ* colitis-related mouse CRC model using azoxymethane (AOM) and dextran sodium sulfate (DSS) [43]. After three cycles treatment of AOM and DSS, the mice were administrated by gavage with SSG or vehicle control at week 7 (Fig. 3A). Again, SSG inhibited *in-situ* CRC growth, which was reflected by that the number of tumors on the colon diminished significantly in SSG-treated group compared to control (Fig. 3B and C). We found that mice weights were slightly reduced during week 10–14 after SSG treatment, but came back at week 15 (Fig. 3D). No signs of cytotoxicity were found in the stomach, liver, kidney, and spleen of SSG treated group, further indicating tolerability of the treatment (Fig. 3E). Likewise, SSG increased the percentage of NEUT% and MONO% while reduced the amount of Lymph% but did not change the counts of other types of leukocytes (Table S3). These data further suggested SSG inhibited tumor growth in an *in-situ* CRC mouse model.

3.4. Transcriptome sequencing analysis suggested that Hmox1 were upregulated by SSG

To find out how SSG inhibits tumor growth and induces cell death, comparative transcriptome sequencing of CT26 cells after DMSO and SSG treatments was carried out. 171 genes were upregulated and 24 genes were downregulated after SSG treatment with the most striking changes found in *Hmox1*, an inducible heme oxygenase which can convert heme to Fe^{2+} to trigger ferroptosis, which upregulated about 73 times (Fig. 4A and B). GO and KEGG analysis of the differentially expressed genes (DEGs) showed that the main changed categories after SSG treatment (Fig. 4C and D), including "Ferroptosis", "Glutathione metabolism", "glutathione binding", and "glutathione transferase activity", which further indicated that ferroptosis were induced. Then, the interactions among the upregulated genes were analyzed by the PPI network (Fig. 4E) and a group of genes directly interact with *Hmox1*, including ferroptosis related *Ptgs2*, *Ddit3*, *Sqstm1* et al. were identified (Fig. 4F). Above results again supported the results in Fig. 1 that ferroptosis was induced by SSG.

3.5. SSG induces Hmox1-mediated ferroptosis in CT26 cells

Because the most striking pathways changed after SSG treatment include the *Hmox1*-mediated ferroptosis pathway, we further analyzed these ferroptosis-related genes by qPCR. In consistent with the RNAseq, SSG treatment induced upregulation of multiple ferroptosis-related genes, including *Hmox1*, *Sqstm1*, *Ddit3*, *IL-6*, *Dusp1* and *Ptgs2* (Fig. 5A). Among these genes, *Hmox1* were upregulated about 30 times after treatment. On the other hand, some ferroptosis inhibitory genes, including *GPX4* and *Nrf2*, which did not show significant differences in RNAseq analysis, were found downregulated after SSG treatment by qPCR analysis (Fig. 5B). These data also suggest SSG induces ferroptosis.

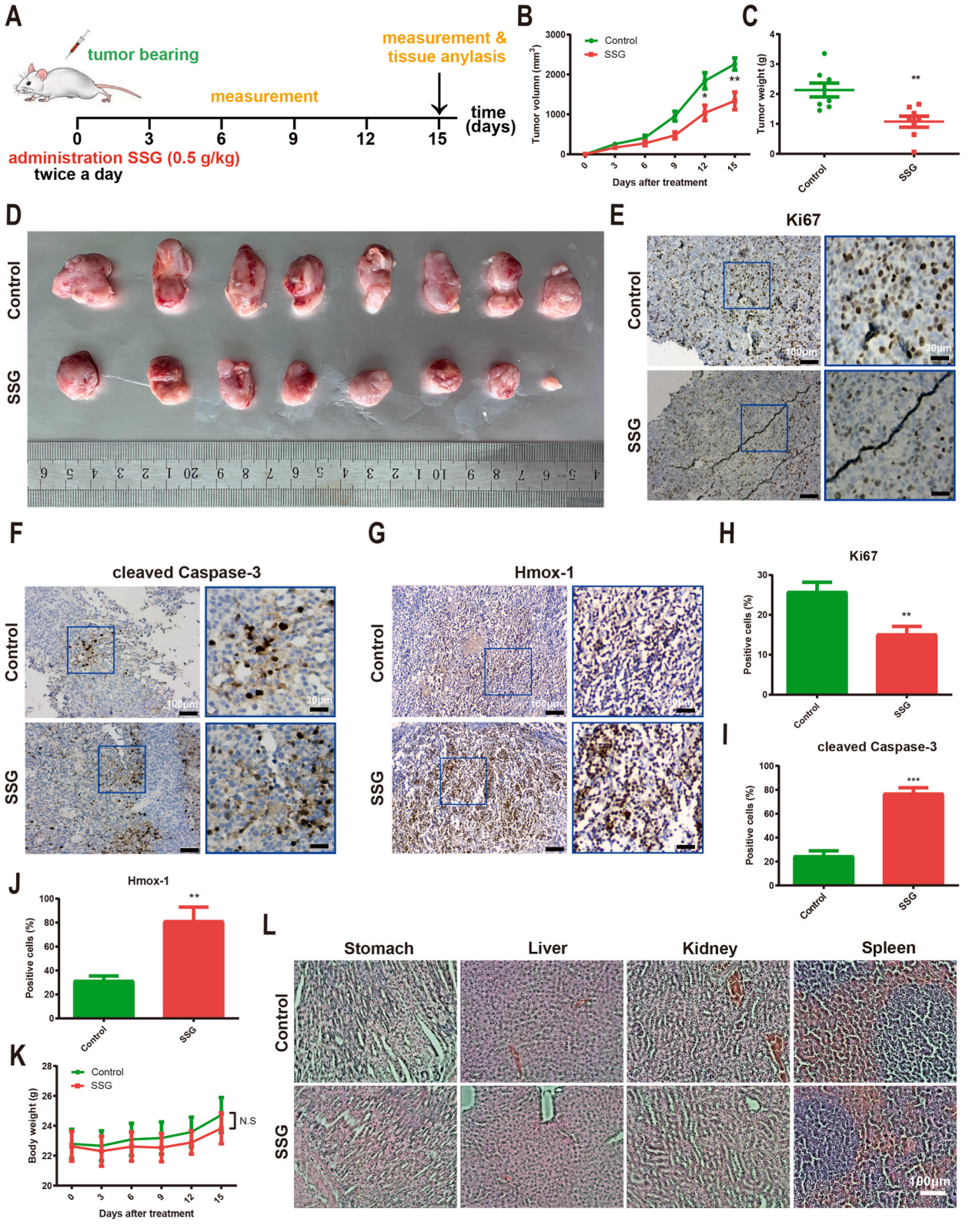

(caption on next page)

Fig. 2. SSG inhibits syngeneic tumor growth *in vivo*. (A) Diagram of this assay. (B–D) Syngeneic tumor volume (B) and weight (C) of each group (n = 8) were analyzed after CT26 tumor-bearing mice were treated with physiological saline or SSG, and tumors were compared at day 15 (D). (E–J) After CT26 tumor-bearing mice treated with physiological saline or SSG for 15 days, the tumor tissues were stained with Ki67 (E,H), cleaved Caspase-3 (F,I), and Hmox-1 (G,J), respectively. The representative staining for Ki67 (E), cleaved Caspase-3 (F), Hmox-1 (G) are shown, and the expression levels of Ki67 (H), cleaved Caspase-3 (I) and Hmox-1 (J) were determined. (K) Mice weight from CT26 tumor-bearing mice treated with physiological saline or SSG were measured at the indicated time points. (L) Stomach, Liver, Kidney and Spleen from CT26 tumor-bearing mice treated with physiological saline or SSG were compared with H&E staining at day 15.

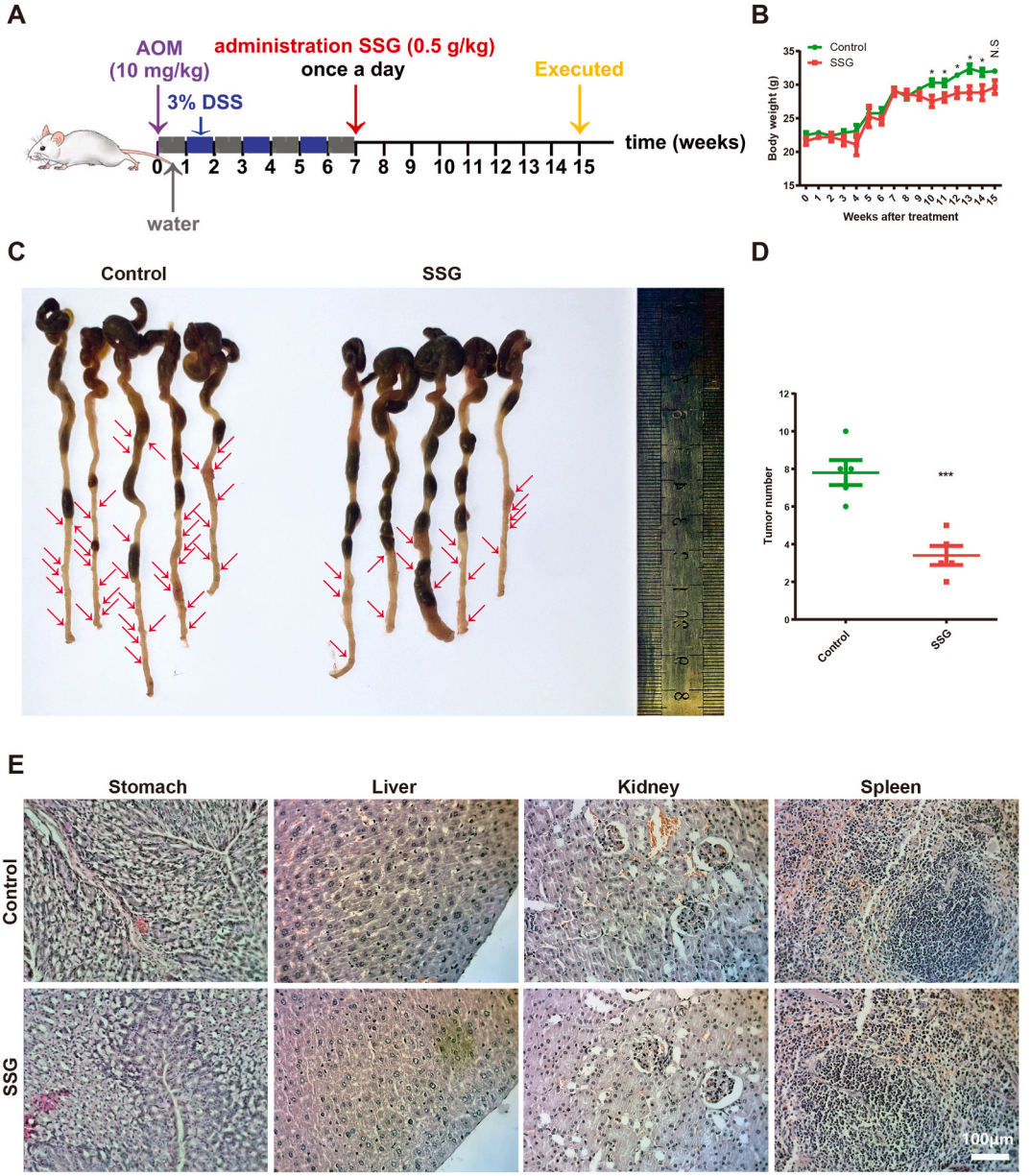

Fig. 3. SSG inhibits an *in-situ* CRC model growth *in vivo*. (A) Diagram of this assay. (B,C) The number of tumors on the colon was counted (B), and pointed by red arrows (C). (D) Mice weight were measured at the indicated time points. (E) Stomach, Liver, Kidney and Spleen from mice treated with physiological saline or SSG were compared with H&E staining at the end of week 15.

To further confirm the ferroptosis induced by SSG in CRC cells, we analyzed several ferroptosis biomarkers. The JC-1 staining assay showed that SSG significantly decreased the ratio of red-fluorescent cells to green-fluorescent cells (Fig. 5C and D), suggesting that SSG treatment disrupted the mitochondrial membrane. Additionally, the fluorescent probe DCFH-DA (2,7-Dichlorodihydrofluorescein

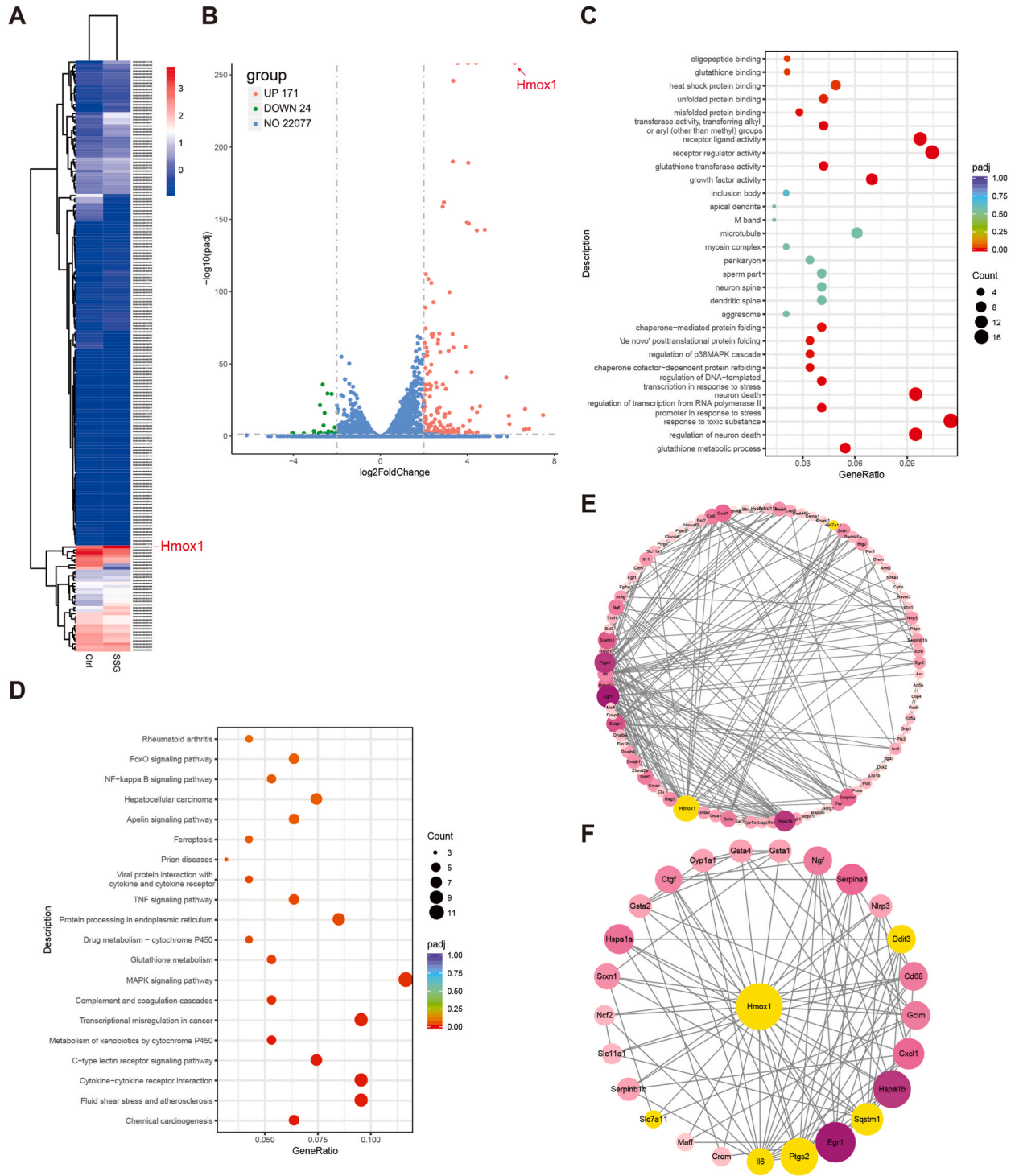

Fig. 4. SSG targets *Hmox-1* to induce ferroptosis. (A) After CT26 cells were treated with SSG or DMSO for 24 h, cells were subjected to transcriptome analysis. (B) Volcano plot of differentially expressed genes (DEGs) of SSG vs DMSO treated group. (C,D) GO (C) and KEGG (D) enrichment analysis of DEGs from SSG vs DMSO treated group. (E,F) PPI network analysis of the upregulated DEGs from SSG vs DMSO (E), and the proteins directly interacts with *Hmox1* were selected and shown (F).

diacetate) was used to detect reactive oxygen species (ROS). As shown in Fig. 5E, SSG increased the generation of ROS and oxidized the DCFH-DA to fluorescent DFC (2,7-Dichlorofluorescein). Subsequently, we conducted a detailed analysis of malondialdehyde (MDA), a biomarker of lipid peroxidation, which is a critical biochemical event in ferroptosis. While MDA is not a specific marker for ferroptosis,

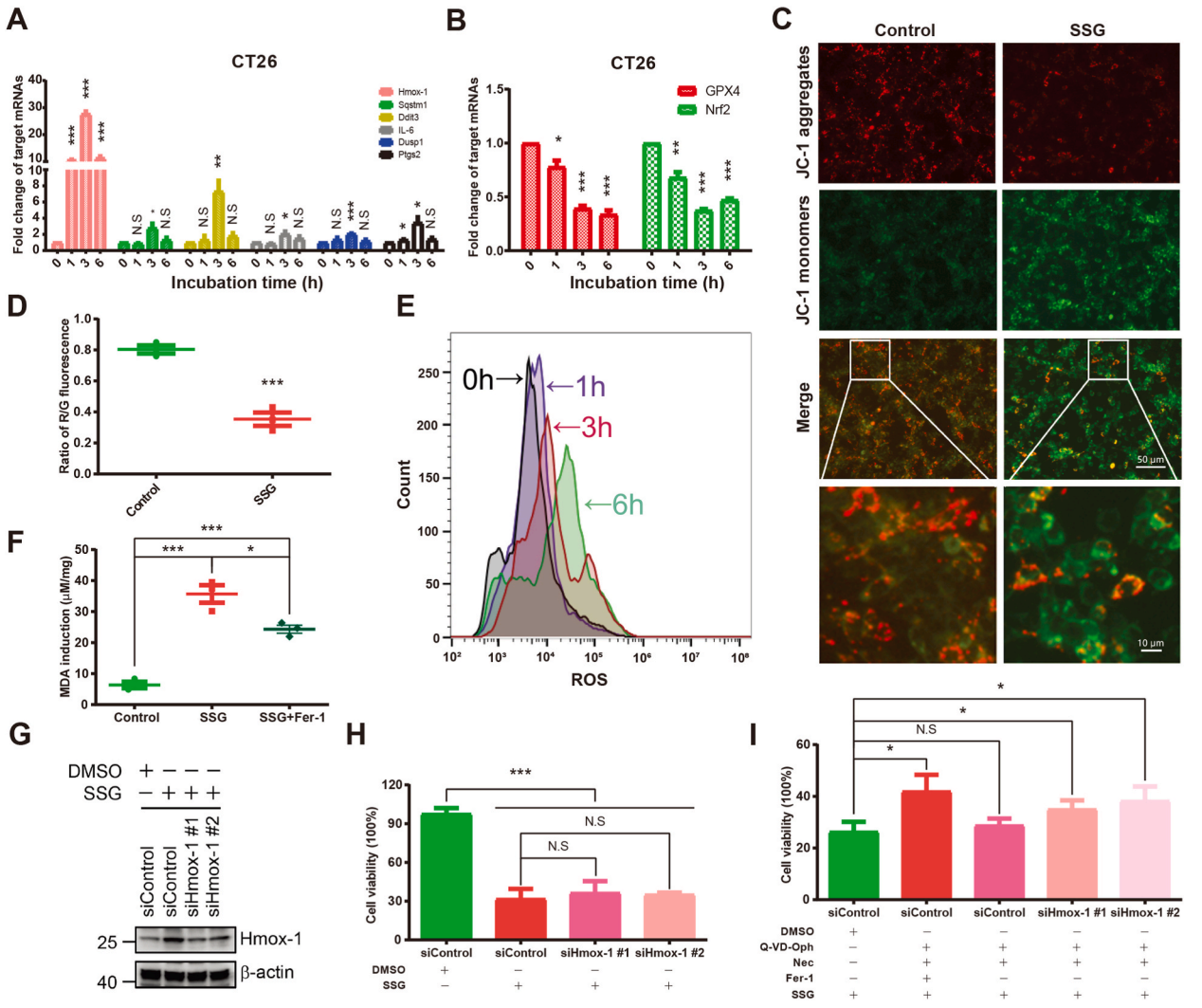

Fig. 5. SSG induces Hmox-1 dependent ferroptosis in CT26 cells. (A,B) After CT26 cells were treated with DMSO or SSG for the indicated time, the ferroptosis related genes were analyzed by qPCR. (C–E) After CT26 cells were treated with DMSO or SSG for the indicated time, cells were stained with JC-1 (C,D) or fluorescent probe DCFH-DA (E) to analyze the change of mitochondrial membrane potential and the level of ROS by fluorescent microscope or flow cytometry, respectively. (F) After a 1-h pre-treatment with or without Fer-1, CT26 cells were exposed to DMSO or SSG for 24 h, after which the MDA levels were measured. (G,H) CT26 cells were transfected with siControl, siHmox-1 #1 or siHmox-1 #2 for 48 h, followed by the addition of either DMSO or SSG for an additional 24 h. Cells were harvested for Hmox-1 detection (G) and viability analysis (H). The original data could be seen in Supplementary Material-Fig. 5G. (I) 48 h post-transfection with siControl or siHmox-1 #1/#2 transfected, cells were pre-treated with the indicated inhibitors for 1 h, and then DMSO or SSG were added for 24 h, after which the viability were measured.

its presence indicates the level of lipid peroxidation, an essential process in the induction of ferroptosis. As shown in Fig. 5F, SSG significantly increased MDA levels, while Fer-1 notably suppressed this increase. However, the inhibitory effect of Fer-1 on SSG-induced MDA levels was not complete compared to the control group, indicating that SSG might induce MDA through multiple pathways. As Hmox-1 upregulation was most significant after SSG treatment, we knocked down Hmox-1 (Fig. 5G) and evaluated the viability of CT26 cells. Interestingly, similar to the effect of Fer-1, Hmox-1 knockdown alone didn't mitigate the cytotoxicity of SSG (Fig. 5H). However, when combined with Q-VD-OPh and Nec, Hmox-1 knockdown significantly enhanced the viability of CT26 cells treated with SSG (Fig. 5I). Taken together, these findings indicate that SSG could induce Hmox-1-dependent ferroptosis in CT26 cells.

3.6. Components of SSG target Hmox1

Previous studies have suggested several treatments or stresses induce ferroptosis through *Hmox1* upregulation [27–29]. To better understand which components of SSG might target *Hmox1*, network pharmacology analysis was used. Through TCMSP database, we obtained 133 active ingredients from six components in SSG and 240 related potential targets. Through analysis of the network of

active ingredients with drug targets (Fig. 6A), Quercetin (MOL000098), Luteolin (MOL000006) and Kaempferol (MOL000422), which are active ingredients of the components Kushen, Huangqi, Gancao and Renshen, were identified to have the ability to target *Hmox1* (Fig. 6B), suggesting a possible mechanism of these components to regulate ferroptosis.

Direct comparison of the Genecards, OMIM and PharmGKB database, 9480 CRC targets were found (Fig. 6C). Among these targets, 7 targets including *Hmox1* were also identified in TCMSP database and SSG upregulated genes (Fig. 6D), indicating a key role of *Hmox1* in the treatment of CRC by SSG.

4. Discussion

Here we report that SSG not only inhibits CRC growth and metastasis *in vitro*, but also inhibits CRC tumor growth in a syngeneic model and an *in-situ* mouse model. Further experiments indicate that SSG upregulates *Hmox1* and several other genes involved in the ferroptosis pathway. Network pharmacology analysis suggests that Quercetin, Luteolin and Kaempferol are the potential active ingredients of SSG to target *Hmox1*. Thus our data suggests that SSG inhibits CRC at least partially through the induction of ferroptosis.

Metastatic or refractory CRCs are often treated with surgery, radiotherapy, chemotherapy, and combined therapies, however, poor prognosis is often seen [1–3]. Fluoropyrimidines, irinotecan, and oxaliplatin are now widely used as chemotherapies for mCRC, while drug resistances have restricted the effects of these therapies. Chemotherapy drugs usually kill tumor cells through apoptosis, and chemotherapy resistance often occurs in the course of treatment because most cancers cells have acquired or intrinsic resistance to apoptosis [44–46]. In contrast to its resistance to apoptosis, cancer cells are more vulnerable to ferroptosis compared to normal cells [19]. Therefore, finding agents to induce other types of tumor cell death such as ferroptosis opens new therapeutic avenues to overcome drug resistance. Quite a few compounds have been reported to induce necroptosis and ferroptosis [47–50]. Previous studies have shown that some Chinese herbal medicines, such as Piperonamide and Tagitin C, inhibit tumor at least partially relies on their ferroptosis-inducing abilities [32–34]. Moreover, Dihydroartemisinin, a derivative of artemisinin, the extract from Artemisia apiacea, increases ROS and reduces glutathione (γ-glutamylcysteinylglycine, GSH) and GPX4 levels in HepG2 cells, resulting ferroptosis through Fenton reaction [51,52]. Pseudolaric acid B, an extract from the root bark of Lysimachia roxburghii, inhibits breast cancer, bladder cancer, cervical cancer, prostate cancer and other malignant tumors by inhibiting system Xc^-, promoting TFR1 expression and

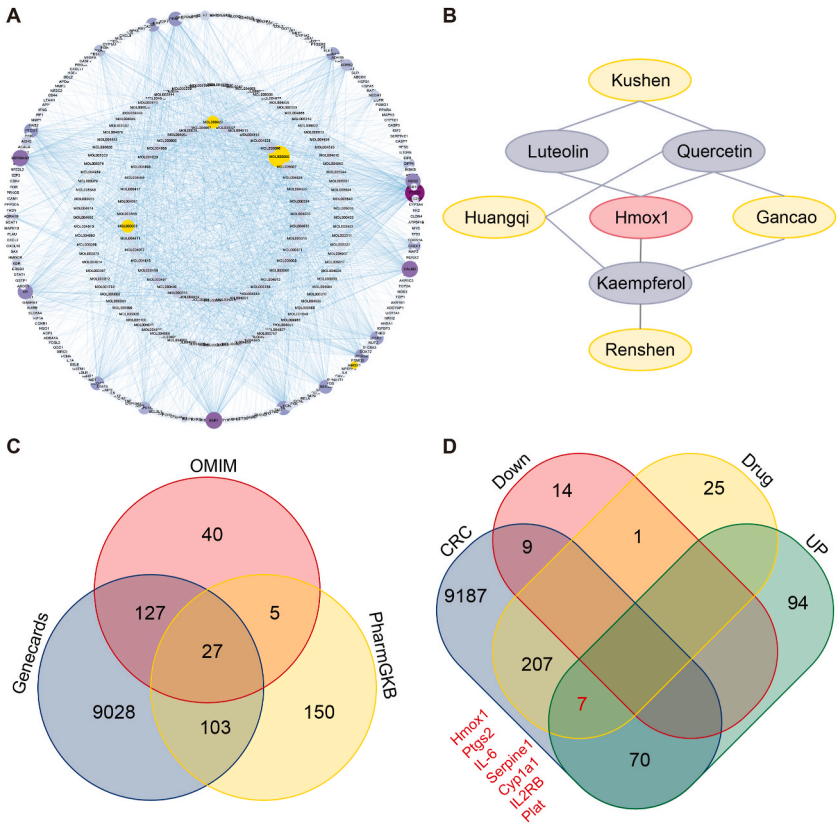

Fig. 6. Components of SSG target *Hmox1*. (A,B) Network analysis of active ingredients of SSG and its potential targets (A), and active ingredients directly targeted *Hmox1* were shown (B). (C) Venn analysis on CRC targets from Genecards, OMIM and PharmGKB. (D) Venn analysis on CRC targets from Genecards, OMIM and PharmGKB, potential targets of SSG from TCMSP and DEGs (upregulated and downregulated) induced by SSG treatment.

increasing the intracellular iron levels, which leads to the accumulation of lipid peroxide and ultimately ferroptosis [53,54].

As a newly elucidated form of programmed cell death, ferroptosis has attracted many research interests. Ferroptosis is different from other types of cell death in several aspects. Morphologically, ferroptotic cells show decreased mitochondria size and mitochondrial cristae and increased thickness of double membrane [20]. Biochemically, ferroptotic cells often have GSH depletion and decreased activity of GPX4, that the lipid oxides in cells were not able to be metabolized by the GPX4 [26,55]. In our study, we found that although the ferroptosis inhibitor Ferrostatin-1 itself did not inhibit SSG-induced cell death, however, when combined with the pan-caspase inhibitor Q-VD-OPh and the necroptosis inhibitor Necrosulfonamide, it reduced SSG-induced cell death significantly. These results suggested SSG induced a mixed type of cell death that composed of apoptosis, necroptosis and ferroptosis. Our further experiments suggested that SSG significantly inhibited CRC cell growth, proliferation and metastasis. And consistent with this, SSG also showed potent tumor inhibition in both subcutaneous syngeneic mouse experiments and AOM/DSS-induced mouse colon cancer model.

Through transcriptome sequencing analysis, we found that SSG upregulated ferroptosis related genes and pathways. In particular, RNAseq analysis suggested that *Hmox1* was upregulated 73 times, some other genes, *Ddit3*, *Ptgs2*, *Sqstm1* et al. were also upregulated. Our further qPCR analysis confirmed that *Hmox1* upregulated about 30 times in the SSG treated group compared to control. Thus, we have focused on the study of SSG-induced ferroptosis. Imbalance of the iron metabolism in cells is one of the major reasons to induce ferroptosis [22,56,57]. While TF/TFR1 complex plays an important role in Fe^{3+} transport, *Hmox1*, the rate limiting enzyme in the process of heme catabolism of iron porphyrin compound, plays a key role in the process of heme decomposition into Fe^{2+}. It was found that doxorubicin can induce Nrf2 dependent up-regulation of *Hmox1* expression in cardiomyocytes, promote the release of free iron ions from heme, and accumulate the cardiomyocytes to induce ferroptosis [58], and our result also found that SSG treatment downregulated the level of Nrf2. However, whether Nrf2 mediates the upregulation of *Hmox1* directly induced by SSG needs to be further estimated.

While it is still very hard to identify the active ingredients that involved in a specific function of Chinese herbal medicine, network pharmacology analysis provides a useful tool based on recent advances in database construction and bioinformatics [59]. We used network pharmacology analysis to find which of the ingredients in SSG related to its ferroptosis induction function and Quercetin, Luteolin and Kaempferol have the ability to target *Hmox1* and induce ferroptosis. And this is consistent with previous report which indicated that Quercetin and Kaempferol may play key role in improving the immune and inflammatory of diabetic kidney disease by affecting ferroptosis [60].

This study provides a new direction for studying the molecular mechanism of action of Chinese herbal compounds. We first determined the tumor-suppression effect of SSG on various cancer cell lines, subcutaneous syngeneic mouse model and AOM/DSS-induced mouse colon cancer model. These all demonstrated that SSG has potential application value in the clinical treatment of CRC. Furthermore, transcriptome sequencing analysis and network pharmacology analysis identified that the active ingredients, Quercetin, Luteolin and Kaempferol, of SSG could target *Hmox1*. However, the specific biological function and mechanisms of these

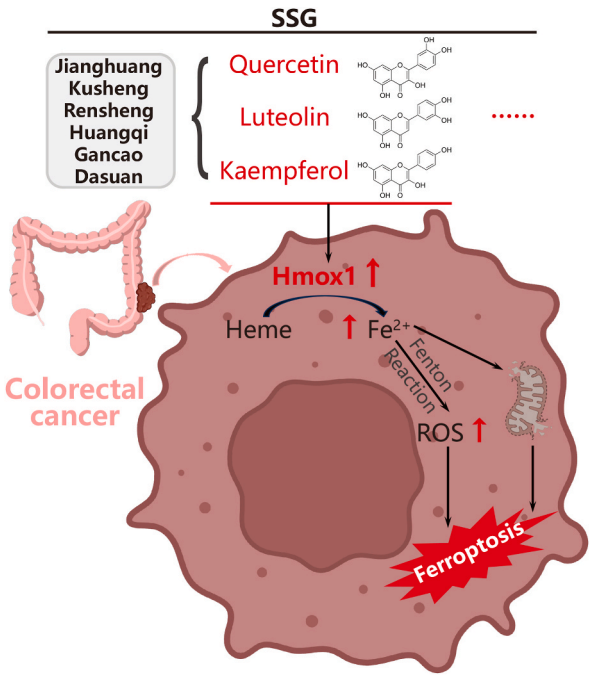

Fig. 7. The schematic summarizes the potential mechanism of SSG's anti-CRC effect. Quercetin, Luteolin and Kaempferol are potential active ingredients of SSG which directly upregulate Hmox-1. Upregulated Hmox-1 promotes the production and accumulation of Fe^{2+} which then induces the accumulation of ROS and the damage of mitochondria, and subsequently activates ferroptosis.

three ingredients on *Hmox1* regulation need to be verified experimentally.

5. Conclusion

In summary, our experiments found that Chinese herbal compound SSG effectively promotes the death of CRC cells and inhibits the proliferation and migration of the cells, while significantly inhibiting the growth of subcutaneous transplanted tumors and *in-situ* induced tumors in mice without damaging the health of mice (Fig. 7). It demonstrated that SSG has potential application value in the clinical treatment of CRC. Further, RNAseq analysis and network pharcological studies suggested that the active ingredients of SSG, including Quercetin, Luteolin and Kaempferol, could target genes such as *Hmox1* to induce iron death in CT26 cells. However, whether and how these active ingredients regulate *Hmox1* and other genes to induce ferroptosis remains to be further clarified.

Ethics declarations

The animal care and study protocols were authorized by the Animal Use and Care Committees at the Hefei Institutes of Physical Science, Chinese Academy of Sciences (approval number, SWYX-DW-2021-74).

Funding

The author(s) declare financial support was received for the research, authorship, and/or publication of this article. This work was supported by the by the Key Scientific Research Project of Wannan Medical College (grant number WK2022Z01), the Wuhu Science and Technology Achievement Transformation Project (grant number 2022cg24), the Natural Science Foundation of the Higher Education Institutions of Anhui Province (grant number 2022AH051223), the Key projects of Anhui Provincial Health Commission (grant number AHWJ2022a002), the Anhui Provincial Department of Education's Scientific Research and Innovation Team (grant number 2023AH010072), the Anhui Provincial Natural Science Foundation (2208085MH221), the National Natural Science Foundation of China (grant number 31970701) and the Anhui Provincial Key R&D Program (grant number 202104a07020007).

Data availability statement

The datasets presented in this study can be found in online repositories, as mentioned in the section of "Materials and Methods". And all data related to this study are available from the corresponding author upon reasonable request.

CRediT authorship contribution statement

Meng Chen: Writing – review & editing, Writing – original draft, Methodology, Formal analysis, Data curation. **Shengli Ma:** Writing – review & editing, Writing – original draft, Supervision, Resources. **Wenbo Ji:** Methodology, Investigation, Formal analysis, Data curation. **Weihua Hu:** Writing – review & editing, Funding acquisition. **Jiguang Gao:** Writing – review & editing, Writing – original draft. **Jianke Yang:** Writing – review & editing, Writing – original draft. **Yu Liu:** Methodology, Formal analysis. **Qianwen Cui:** Methodology, Formal analysis. **Shasha Yang:** Methodology. **Xiaohui Xu:** Writing – review & editing, Writing – original draft, Funding acquisition, Formal analysis. **Haiming Dai:** Writing – review & editing, Writing – original draft, Supervision, Resources, Funding acquisition. **Lei Hu:** Writing – review & editing, Writing – original draft, Project administration, Methodology, Investigation, Funding acquisition, Formal analysis, Data curation, Conceptualization.

Declaration of competing interest

The authors declare that they have no known competing financial interests or personal relationships that could have appeared to influence the work reported in this paper.

Appendix A. Supplementary data

Supplementary data to this article can be found online at https://doi.org/10.1016/j.heliyon.2024.e38021.

References

[1] H. Sung, J. Ferlay, R.L. Siegel, M. Laversanne, I. Soerjomataram, A. JemalF. Bray, Global cancer statistics 2020: GLOBOCAN estimates of incidence and mortality worldwide for 36 cancers in 185 countries, Ca - Cancer J. Clin. 71 (3) (2021) 209–249, https://doi.org/10.3322/caac.21660.

[2] M. Arnold, M.S. Sierra, M. Laversanne, I. Soerjomataram, A. JemalF. Bray, Global patterns and trends in colorectal cancer incidence and mortality, Gut 66 (4) (2017) 683–691, https://doi.org/10.1136/gutjnl-2015-310912.

[3] E. Dekker, P.J. Tanis, J.L.A. Vleugels, P.M. KasiM, B. Wallace, Colorectal cancer, Lancet 394 (10207) (2019) 1467–1480, https://doi.org/10.1016/s0140-6736(19)32319-0.

[4] S. Vodenkova, T. Buchler, K. Cervena, V. Veskrnova, P. VodickaV. Vymetalkova, 5-fluorouracil and other fluoropyrimidines in colorectal cancer: past, present and future, Pharmacol. Ther. 206 (2020) 107447, https://doi.org/10.1016/j.pharmthera.2019.107447.

[5] B. Glimelius, S. Stintzing, J. Marshall, T. YoshinoA. de Gramont, Metastatic colorectal cancer: advances in the folate-fluoropyrimidine chemotherapy backbone, Cancer Treat Rev. 98 (2021) 102218, https://doi.org/10.1016/j.ctrv.2021.102218.

[6] P. RieraD. Páez, Elucidating the role of pharmacogenetics in irinotecan efficacy and adverse events in metastatic colorectal cancer patients, Expet Opin. Drug Metabol. Toxicol. 17 (10) (2021) 1157–1163, https://doi.org/10.1080/17425255.2021.1974397.

[7] G. Tonini, M. Imperatori, B. Vincenzi, A.M. FrezzaD. Santini, Rechallenge therapy and treatment holiday: different strategies in management of metastatic colorectal cancer, J. Exp. Clin. Cancer Res. 32 (1) (2013) 92, https://doi.org/10.1186/1756-9966-32-92.

[8] F.F. Qi, Y. Yang, H. ZhangH. Chen, Long non-coding RNAs: key regulators in oxaliplatin resistance of colorectal cancer, Biomed. Pharmacother. 128 (2020) 110329, https://doi.org/10.1016/j.biopha.2020.110329.

[9] K.K. Iyer, N.P. van Erp, D.V.F. Tauriello, H.M. W. VerheulD. Poel, Lost in translation: revisiting the use of tyrosine kinase inhibitors in colorectal cancer, Cancer Treat Rev. 110 (2022) 102466, https://doi.org/10.1016/j.ctrv.2022.102466.

[10] G. Giordano, P. Parcesepe, G. Bruno, A. Piscazzi, V. Lizzi, A. Remo, M. Pancione, M.R. D'Andrea, E. De Santis, L. Coppola, et al., Evidence-based second-line treatment in RAS wild-type/mutated metastatic colorectal cancer in the precision medicine era, Int. J. Mol. Sci. 22 (2021) 14, https://doi.org/10.3390/ijms22147717.

[11] S. PiawahA, P. Venook, Targeted therapy for colorectal cancer metastases: a review of current methods of molecularly targeted therapy and the use of tumor biomarkers in the treatment of metastatic colorectal cancer, Cancer 125 (23) (2019) 4139–4147, https://doi.org/10.1002/cncr.32163.

[12] E. Wensink, M. Bond, E. Kucukkose, A. May, G. Vink, M. Koopman, O. KranenburgJ. Roodhart, A review of the sensitivity of metastatic colorectal cancer patients with deficient mismatch repair to standard-of-care chemotherapy and monoclonal antibodies, with recommendations for future research, Cancer Treat Rev. 95 (2021) 102174, https://doi.org/10.1016/j.ctrv.2021.102174.

[13] D.Y. Lizardo, C. Kuang, S. Hao, J. Yu, Y. HuangL. Zhang, Immunotherapy efficacy on mismatch repair-deficient colorectal cancer: from bench to bedside, Biochim. Biophys. Acta Rev. Canc 1874 (2) (2020) 188447, https://doi.org/10.1016/j.bbcan.2020.188447.

[14] D.T. Le, J.N. Durham, K.N. Smith, H. Wang, B.R. Bartlett, L.K. Aulakh, S. Lu, H. Kemberling, C. Wilt, B.S. Luber, et al., Mismatch repair deficiency predicts response of solid tumors to PD-1 blockade, Science 357 (6349) (2017) 409–413, https://doi.org/10.1126/science.aan6733.

[15] M.Y. Kong, L.Y. Li, Y.M. Lou, H.Y. ChiJ. Wu, Chinese herbal medicines for prevention and treatment of colorectal cancer: from molecular mechanisms to potential clinical applications, J Integr Med 18 (5) (2020) 369–384, https://doi.org/10.1016/j.joim.2020.07.005.

[16] Y. Fan, Z. Ma, L. Zhao, W. Wang, M. Gao, X. Jia, H. OuyangJ. He, Anti-tumor activities and mechanisms of Traditional Chinese medicines formulas: a review, Biomed. Pharmacother. 132 (2020) 110820, https://doi.org/10.1016/j.biopha.2020.110820.

[17] W.J. Huang, S. Ruan, F. Wen, X.N. Lu, S.P. Gu, X.X. Chen, M. LiuP. Shu, Multidrug resistance of gastric cancer: the mechanisms and Chinese medicine reversal agents, Cancer Manag. Res. 12 (2020) 12385–12394, https://doi.org/10.2147/cmar.S274599.

[18] K. Li, K. Xiao, S. Zhu, Y. WangW. Wang, Chinese herbal medicine for primary liver cancer therapy: perspectives and challenges, Front. Pharmacol. 13 (2022) 889799, https://doi.org/10.3389/fphar.2022.889799.

[19] B. Hassannia, P. VandenabeeleT, Vanden berghe, targeting ferroptosis to iron out cancer, Cancer Cell 35 (6) (2019) 830–849, https://doi.org/10.1016/j.ccell.2019.04.002.

[20] S.J. Dixon, K.M. Lemberg, M.R. Lamprecht, R. Skouta, E.M. Zaitsev, C.E. Gleason, D.N. Patel, A.J. Bauer, A.M. Cantley, W.S. Yang, et al., Ferroptosis: an iron-dependent form of nonapoptotic cell death, Cell 149 (5) (2012) 1060–1072, https://doi.org/10.1016/j.cell.2012.03.042.

[21] J. Zou, L. Wang, H. Tang, X. Liu, F. PengC. Peng, Ferroptosis in non-small cell lung cancer: progression and therapeutic potential on it, Int. J. Mol. Sci. 22 (2021) 24, https://doi.org/10.3390/ijms222413335.

[22] G. Lei, L. ZhuangB. Gan, Targeting ferroptosis as a vulnerability in cancer, Nat. Rev. Cancer 22 (7) (2022) 381–396, https://doi.org/10.1038/s41568-022-00459-0.

[23] B.R. Stockwell, Ferroptosis turns 10: emerging mechanisms, physiological functions, and therapeutic applications, Cell 185 (14) (2022) 2401–2421, https://doi.org/10.1016/j.cell.2022.06.003.

[24] D. Liang, A.M. MinikesX. Jiang, Ferroptosis at the intersection of lipid metabolism and cellular signaling, Mol. Cell. 82 (12) (2022) 2215–2227, https://doi.org/10.1016/j.molcel.2022.03.022.

[25] X. Song, Y. Xie, R. Kang, W. Hou, X. Sun, M.W. Epperly, J.S. GreenbergerD. Tang, FANCD2 protects against bone marrow injury from ferroptosis, Biochem. Biophys. Res. Commun. 480 (3) (2016) 443–449, https://doi.org/10.1016/j.bbrc.2016.10.068.

[26] W.S. YangB, R. Stockwell, Synthetic lethal screening identifies compounds activating iron-dependent, nonapoptotic cell death in oncogenic-RAS-harboring cancer cells, Chem. Biol. 15 (3) (2008) 234–245, https://doi.org/10.1016/j.chembiol.2008.02.010.

[27] Z. Tang, Y. Ju, X. Dai, N. Ni, Y. Liu, D. Zhang, H. Gao, H. Sun, J. ZhangP. Gu, HO-1-mediated ferroptosis as a target for protection against retinal pigment epithelium degeneration, Redox Biol. 43 (2021) 101971, https://doi.org/10.1016/j.redox.2021.101971.

[28] A.V. Menon, J. Liu, H.P. Tsai, L. Zeng, S. Yang, A. AsnaniJ. Kim, Excess heme upregulates heme oxygenase 1 and promotes cardiac ferroptosis in mice with sickle cell disease, Blood 139 (6) (2022) 936–941, https://doi.org/10.1182/blood.2020008455.

[29] X. Lai, Y. Sun, X. Zhang, D. Wang, J. Wang, H. Wang, Y. Zhao, X. Liu, X. Xu, H. Song, et al., Honokiol induces ferroptosis by upregulating HMOX1 in acute myeloid leukemia cells, Front. Pharmacol. 13 (2022) 897791, https://doi.org/10.3389/fphar.2022.897791.

[30] W.S. Yang, K.J. Kim, M.M. Gaschler, M. Patel, M.S. ShchepinovB, R. Stockwell, Peroxidation of polyunsaturated fatty acids by lipoxygenases drives ferroptosis, Proc. Natl. Acad. Sci. U.S.A. 113 (34) (2016) E4966–E4975, https://doi.org/10.1073/pnas.1603244113.

[31] W.S. Yang, R. SriRamaratnam, M.E. Welsch, K. Shimada, R. Skouta, V.S. Viswanathan, J.H. Cheah, P.A. Clemons, A.F. Shamji, C.B. Clish, et al., Regulation of ferroptotic cancer cell death by GPX4, Cell 156 (1–2) (2014) 317–331, https://doi.org/10.1016/j.cell.2013.12.010.

[32] Y. Yamaguchi, T. KasukabeS. Kumakura, Piperlongumine rapidly induces the death of human pancreatic cancer cells mainly through the induction of ferroptosis, Int. J. Oncol. 52 (3) (2018) 1011–1022, https://doi.org/10.3892/ijo.2018.4259.

[33] D. Basak, S.R. PunganuruK, S. Srivenugopal, Piperlongumine exerts cytotoxic effects against cancer cells with mutant p53 proteins at least in part by restoring the biological functions of the tumor suppressor, Int. J. Oncol. 48 (4) (2016) 1426–1436, https://doi.org/10.3892/ijo.2016.3372.

[34] R. Wei, Y. Zhao, J. Wang, X. Yang, S. Li, Y. Wang, X. Yang, J. Fei, X. Hao, Y. Zhao, et al., Tagitinin C induces ferroptosis through PERK-Nrf2-HO-1 signaling pathway in colorectal cancer cells, Int. J. Biol. Sci. 17 (11) (2021) 2703–2717, https://doi.org/10.7150/ijbs.59404.

[35] L. Ye, F. Jin, S.K. KumarY. Dai, The mechanisms and therapeutic targets of ferroptosis in cancer, Expert Opin. Ther. Targets 25 (11) (2021) 965–986, https://doi.org/10.1080/14728222.2021.2011206.

[36] Q. Sun, M. He, M. Zhang, S. Zeng, L. Chen, H. Zhao, H. Yang, M. Liu, S. RenH. Xu, Traditional Chinese medicine and colorectal cancer: implications for drug discovery, Front. Pharmacol. 12 (2021) 685002, https://doi.org/10.3389/fphar.2021.685002.

[37] Z.J. Yang, S.Y. Huang, D.D. Zhou, R.G. Xiong, C.N. Zhao, A.P. Fang, Y.J. Zhang, H.B. LiH, L. Zhu, Effects and mechanisms of curcumin for the prevention and management of cancers: an updated review, Antioxidants 11 (2022) 8, https://doi.org/10.3390/antiox11081481.

[38] X. He, J. Fang, L. Huang, J. WangX. Huang, Sophora flavescens Ait, Traditional usage, phytochemistry and pharmacology of an important traditional Chinese medicine, J. Ethnopharmacol. 172 (2015) 10–29, https://doi.org/10.1016/j.jep.2015.06.010.

[39] J. Li, F. LiD. Jin, Ginsenosides are promising medicine for tumor and inflammation: a review, Am. J. Chin. Med. 51 (4) (2023) 883–908, https://doi.org/10.1142/s0192415x23500416.

[40] X. Lai, W. Xia, J. WeiX. Ding, Therapeutic effect of Astragalus polysaccharides on hepatocellular carcinoma H22-bearing mice, Dose Response 15 (1) (2017) 1559325816685182, https://doi.org/10.1177/1559325816685182.

[41] Z.H. Tang, T. Li, Y.G. Tong, X.J. Chen, X.P. Chen, Y.T. WangJ. Lu, A systematic review of the anticancer properties of compounds isolated from licorice (Gancao), Planta Med. 81 (18) (2015) 1670–1687, https://doi.org/10.1055/s-0035-1558227.

[42] A. Samy, D. Shah, P. Shahagadkar, H. ShahG. Munirathinam, Can diallyl trisulfide, a dietary garlic-derived compound, activate ferroptosis to overcome therapy resistance in prostate cancer? Nutr. Health 28 (2) (2022) 207–212, https://doi.org/10.1177/02601060211018360.
[43] T. Tanaka, H. Kohno, R. Suzuki, Y. Yamada, S. SugieH. Mori, A novel inflammation-related mouse colon carcinogenesis model induced by azoxymethane and dextran sodium sulfate, Cancer Sci. 94 (11) (2003) 965–973, https://doi.org/10.1111/j.1349-7006.2003.tb01386.x.
[44] C. Holohan, S. Van Schaeybroeck, D.B. LongleyP, G. Johnston, Cancer drug resistance: an evolving paradigm, Nat. Rev. Cancer 13 (10) (2013) 714–726, https://doi.org/10.1038/nrc3599.
[45] C. Zhang, X. Liu, S. Jin, Y. ChenR. Guo, Ferroptosis in cancer therapy: a novel approach to reversing drug resistance, Mol. Cancer 21 (1) (2022) 47, https://doi.org/10.1186/s12943-022-01530-y.
[46] P. SinghB. Lim, Targeting apoptosis in cancer, Curr. Oncol. Rep. 24 (3) (2022) 273–284, https://doi.org/10.1007/s11912-022-01199-y.
[47] K. Mortezaee, E. Salehi, H. Mirtavoos-Mahyari, E. Motevaseli, M. Najafi, B. Farhood, R.J. RosengrenA. Sahebkar, Mechanisms of apoptosis modulation by curcumin: implications for cancer therapy, J. Cell. Physiol. 234 (8) (2019) 12537–12550, https://doi.org/10.1002/jcp.28122.
[48] B.W. Jiang, W.J. Zhang, Y. Wang, L.P. Tan, Y.L. Bao, Z.B. Song, C.L. Yu, S.Y. Wang, L. LiuY, X. Li, Convallatoxin induces HaCaT cell necroptosis and ameliorates skin lesions in psoriasis-like mouse models, Biomed. Pharmacother. 121 (2020) 109615, https://doi.org/10.1016/j.biopha.2019.109615.
[49] L. Liu, J. Fan, G. Ai, J. Liu, N. Luo, C. LiZ. Cheng, Berberine in combination with cisplatin induces necroptosis and apoptosis in ovarian cancer cells, Biol. Res. 52 (1) (2019) 37, https://doi.org/10.1186/s40659-019-0243-6.
[50] Y. Mou, J. Wang, J. Wu, D. He, C. Zhang, C. DuanB. Li, Ferroptosis, a new form of cell death: opportunities and challenges in cancer, J. Hematol. Oncol. 12 (1) (2019) 34, https://doi.org/10.1186/s13045-019-0720-y.
[51] Z. Wang, M. Li, Y. Liu, Z. Qiao, T. Bai, L. YangB. Liu, Dihydroartemisinin triggers ferroptosis in primary liver cancer cells by promoting and unfolded protein response-induced upregulation of CHAC1 expression, Oncol. Rep. 46 (2021) 5, https://doi.org/10.3892/or.2021.8191.
[52] Z. Cui, H. Wang, S. Li, T. Qin, H. Shi, J. Ma, L. Li, G. Yu, T. JiangC. Li, Dihydroartemisinin enhances the inhibitory effect of sorafenib on HepG2 cells by inducing ferroptosis and inhibiting energy metabolism, J. Pharmacol. Sci. 148 (1) (2022) 73–85, https://doi.org/10.1016/j.jphs.2021.09.008.
[53] Z. Wang, Y. Ding, X. Wang, S. Lu, C. Wang, C. He, L. Wang, M. Piao, G. Chi, Y. Luo, et al., Pseudolaric acid B triggers ferroptosis in glioma cells via activation of Nox 4 and inhibition of xCT, Cancer Lett. 428 (2018) 21–33, https://doi.org/10.1016/j.canlet.2018.04.021.
[54] X. Wu, H. Sheng, L. Zhao, M. Jiang, H. Lou, Y. Miao, N. Cheng, W. Zhang, D. DingW. Li, Co-loaded lapatinib/PAB by ferritin nanoparticles eliminated ECM-detached cluster cells via modulating EGFR in triple-negative breast cancer, Cell Death Dis. 13 (6) (2022) 557, https://doi.org/10.1038/s41419-022-05007-0.
[55] J.P. Friedmann Angeli, M. Schneider, B. Proneth, Y.Y. Tyurina, V.A. Tyurin, V.J. Hammond, N. Herbach, M. Aichler, A. Walch, E. Eggenhofer, et al., Inactivation of the ferroptosis regulator Gpx4 triggers acute renal failure in mice, Nat. Cell Biol. 16 (12) (2014) 1180–1191, https://doi.org/10.1038/ncb3064.
[56] X. Fang, H. Ardehali, J. MinF. Wang, The molecular and metabolic landscape of iron and ferroptosis in cardiovascular disease, Nat. Rev. Cardiol. 20 (1) (2023) 7–23, https://doi.org/10.1038/s41569-022-00735-4.
[57] X. Jiang, B.R. StockwellM. Conrad, Ferroptosis: mechanisms, biology and role in disease, Nat. Rev. Mol. Cell Biol. 22 (4) (2021) 266–282, https://doi.org/10.1038/s41580-020-00324-8.
[58] X. Fang, H. Wang, D. Han, E. Xie, X. Yang, J. Wei, S. Gu, F. Gao, N. Zhu, X. Yin, et al., Ferroptosis as a target for protection against cardiomyopathy, Proc. Natl. Acad. Sci. U.S.A. 116 (7) (2019) 2672–2680, https://doi.org/10.1073/pnas.1821022116.
[59] R. Zhang, X. Zhu, H. BaiK. Ning, Network pharmacology databases for traditional Chinese medicine: review and assessment, Front. Pharmacol. 10 (2019) 123, https://doi.org/10.3389/fphar.2019.00123.
[60] J. Ma, C. Li, T. Liu, L. Zhang, X. Wen, X. LiuW. Fan, Identification of markers for diagnosis and treatment of diabetic kidney disease based on the ferroptosis and immune, Oxid. Med. Cell. Longev. 2022 (2022) 9957172, https://doi.org/10.1155/2022/9957172.